J Mater Sci (2007) 42:4581–4590
DOI 10.1007/s10853-006-0560-3

Microstructural characterisation by X-ray scattering of perovskite-type $La_{0.8}Sr_{0.2}MnO_{3\pm\delta}$ thin films prepared by a dip-coating process

P. Lenormand · A. Lecomte · C. Laberty-Robert · F. Ansart · A. Boulle

Received: 13 May 2005 / Accepted: 13 June 2006 / Published online: 16 February 2007

Abstract The $La_{0.8}Sr_{0.2}MnO_3$ (LSM) cathode materials are widely used in solid oxide fuel cells (SOFCs) as electronic conductors. In such materials, the reduction of oxygen is located at the triple contact boundaries: air/cathode LSM/electrolyte which is generally Yttria Stabilised Zirconia (YSZ). In order to improve the chemical reactions at these air/cathode LSM/electrolyte interfaces, the triple phase boundary length has to be optimised. In this aim, we have first synthesised the $La_{0.8}Sr_{0.2}MnO_3$ phase by a sol–gel route and, second, LSM thin films have been deposited on various polished substrates by using a dip-coating process. The structure and microstructure of the resulting LSM thin layers have been investigated by using well suited complementary techniques such as X-ray reflectometry, grazing incidence small angle X-ray scattering, X-ray diffraction and scanning electronic microscopy. The structural and microstructural parameters of LSM thin films have been managed and studied as a function of synthesis parameters such as initial metallic salt concentration, time and temperature of annealing. The higher the metallic salt concentration, the higher the thickness of the film, the smaller the film density. The as-prepared layers are amorphous and the single crystallised perovskite form is obtained for low temperature heat treatments. Therefore, the annealed coatings are constituted by randomly oriented LSM nanocrystals, which organise in a more or less dense close-packed microstructure according to the initial metallic salt concentration.

P. Lenormand (✉) · C. Laberty-Robert · F. Ansart
Centre Inter-universitaire de Recherche et d'Ingénierie sur les MATériaux, UMR 5085, Université Paul Sabatier, Bât. 2R1-118 route de Narbonne, 31062 Toulouse Cedex 4, France
e-mail: lenorman@chimie.ups-tlse.fr

A. Lecomte · A. Boulle
Science des Procédés Céramiques et Traitements de Surface, UMR 6638-CNRS ENSCI, 47-73 Avenue Albert Thomas, 87065 Limoges Cedex, France

Introduction

Solid oxide fuel cells (SOFCs) are solid electrical energy conversion devices with high efficiency and low pollution [1, 2]. Strontium-doped lanthanum manganite, $La_{0.8}Sr_{0.2}MnO_{3\pm\delta}$ (LSM), is known to be a very promising cathode material for SOFCs [3]. Nowadays, their operating temperature is about 1,000 °C. To lower the working temperature around 700 °C, the interfacial cathode/electrolyte resistances have to be decreased by a better control of the material microstructure. Indeed, the microstructure of the porous electrodes is critical for the performances of a SOFC since it affects the cathode reduction of oxygen and the chemical reactions at the air/electrode/electrolyte interface commonly denoted as the triple phase boundary (TPB) interface [4]. To prepare a highly active air electrode, the length of TPB for the electrode reactions has to be sufficient and optimised by designing the microstructure of the porous air electrode so as not to disturb the adsorbed oxygen surface diffusion on the electrode.

The preparation of these compounds by chemical methods, such as citrate-gel process [5], co-precipitation

techniques [6], combustion [7] and auto-ignition [8] processes have been attempted. In this study, the Pechini method [9] is further modified to elaborate $La_{0.8}Sr_{0.2}MnO_{3\pm\delta}$ oxide thin films. This polymeric route has been proved to lead to the formation of complex oxides with highly homogeneous fine particles at low temperature. Moreover, the interest of this derived sol–gel route to elaborate thin films by a dip-coating process is unquestionable mainly because with such a process, the constitutive matter of the coating is globally deposited and after an adapted thermal treatment, the material and its shaping are simultaneously obtained [10].

Both formation and transformation mechanisms studies of thin films synthesised by the sol–gel route are most recent and not often carried out by the use of several complementary non-destructive and statistical experimental techniques such as X-ray scattering measurements. As it has been shown for zirconia (ZrO_2) sol–gel thin films elaborated by the alkoxide route, numerous microstructural information on a nanometric scale of such sol–gel layers, as thickness, particle shape and size, interparticle distance or correlation length... have been obtained by combination of the experimental techniques as X-ray reflectivity (XRR), X-ray diffraction (XRD) and grazing incidence small angle X-ray scattering (GISAXS) [11, 12].

In the present work, we aim to show that microstructural analysis by X-ray scattering experiments of LSM thin layers obtained via a derived Pechini process can be performed and the resultant microstructure of films controlled from the sol synthesis parameters and heat treatment conditions.

Experimental

Sample preparation

All the sols employed for the thin layers synthesis corresponding to $La_{0.8}Sr_{0.2}MnO_{3\pm\delta}$ phase are prepared by using a polymeric route developed and previously described by Gaudon et al. [13, 14]. Pure metal nitrates, $La(NO_3) \cdot 6H_2O$, $Sr(NO_3)_2$, $Mn(NO_3)_2 \cdot 4H_2O$ are used as precursors. They are weighted at the LSM molar composition and dissolved in a minimum distilled water amount under mechanical stirring. The resulting solution is added to a polymeric mixture constituted by both hexametylenetetramine (HMTA) and acetylacetone (acac) which are required as polymerisant and chelating agents for the process, respectively. Then, the initial metallic salt concentration of the sol is controlled and fixed by the addition of acetic acid (CH_3COOH), used as solvent. Heating at 80–90 °C promotes both polymerisation and polycondensation reactions leading to increase the viscosity of the solution. Finally, the viscosity is systematically adjusted at about 40 mPa·s at ambient temperature.

Therefore, different coatings of LSM precursor are carried out by using a dip-coating process under ambient conditions for various metallic salt concentrations ranging from 0.08 to 0.6 mol/l on both (100) Si single crystals and polished mirror Yttria Stabilised Zirconia (YSZ) polycrystalline substrates which are previously cleaned in successive ultrasonic baths of acetone and alcohol [15]. The withdrawal speed of the step-by-step dipping–withdrawing apparatus is constant and adjusted at 1.7 cm/min. Based on previous studies on LSM powders and thin films synthesised by this organic route, the optimal heat treatment to fire the samples is 700 °C during 2 h in air with a heating rate of 100 °C/h [14].

X-ray specular reflectivity

The thickness, density and roughness of interfaces as defined by Nevot et al. [16] of LSM thin layers have been measured by X-ray specular reflectivity (XRR), a non-destructive technique particularly suitable for their investigation. The reflectivity data are collected by means of an original angular dispersive reflectometer [11] initially developed by Naudon et al. [17]. All reflected beams are simultaneously recorded by using a linear position sensitive detector (INEL LPS 50-France). As previously described, advantages in the use of this original apparatus lie in the fact that no movement of both the sample and the detector is necessary during the measurement. The exposure time to data recording is obviously considerably diminished, typically about 3 h.

The microstructural parameters are obtained by fitting the experimental XRR data by using a modified Fresnel recursive formula, generally referred as the Parratt formalism [18]. Both nanometer-scale surface and interface roughnesses are described by a Debye-Waller like damping term as introduced by Névot et al. [16, 19] in the calculation of the Fresnel coefficients and defined as the root means square (r.m.s.).

Grazing incidence small-angle X-ray scattering

The Grazing Incidence Small Angle X-ray Scattering (GISAXS) measurements have been performed by using a conventional laboratory Small Angle X-ray

Scattering (SAXS) experimental set-up with a point like collimation geometry, modified and adapted to the case of grazing incidence [11]. The sample holder is equipped with both two translations and one step-by-step rotation with optical encoder, which allows a very precise surface sample adjustment in the direct beam and the control of the incident angle. The scattered intensity is recorded using a linear position sensitive detector (Physique et Industrie, Elphyse Department-France) which is positioned parallel to the surface sample. Its height position is precisely controlled and adjusted slightly below the reflected beam I_r (Fig. 1), which is masked by a lead beam stop set along the vertical axis.

The apparatus setting both to position the sample accordingly to the X-ray beam and to determine the sample angular origin is classically made [20]. To totally penetrate the coating, the grazing angle of the incident beam, I_i, on the sample surface must be slightly larger than the layer critical angle α_c, α_c being previously measured by X-ray reflectivity. So the transmitted beam, I_t, goes through the layer and acts as a primary beam to give rise to a SAXS signal [21–23]. However, less than the upper half part of the GISAXS pattern can be recorded (Fig. 1).

The origin of the reciprocal space is the point O which position is calculated according to the incident angle α and the refraction index of the coating as determined from the XRR curves. Then, the GISAXS data are corrected for refraction and absorption effects before analysis [24]. Finally, the scattered intensity I(q) is presented as a function of the modulus of the scattering vector $\boldsymbol{q}$ which is given by $q = 4\pi\sin(\theta)/\lambda$ where θ is half the scattering angle and λ the wavelength of the incident radiation ($CuK_{\alpha 1}$ radiation). Two sample-detector distances of 0.5 and 1.5 m are used in order to cover a q-range from about 0.3 to 4.0 nm^{-1}. Thus, in such experimental conditions, the measurable scattering particle sizes or interparticles distances range from 1.5–2 to about 25 nm.

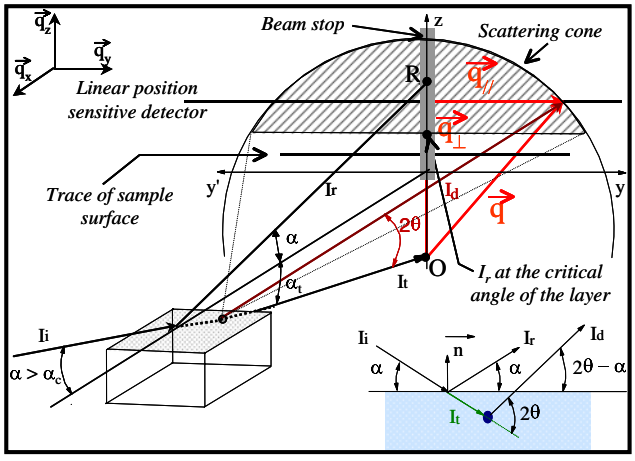

Fig. 1 Experimental geometry for GISAXS measurements. α and α_t are the incidence and transmitted angles, respectively. I_t, I_r and I_d are the transmitted, reflected and diffused beams. 2θ is the scattering angle

X-ray diffraction

X-ray diffraction (XRD) was used to determine the nature of the crystalline phases and more particularly to check that the layers are crystallised as single perovskite phase. The as-prepared and annealed LSM thin films are investigated by asymmetric X-rays diffraction measurements on a Debye-Scherrer type apparatus operating on flat samples [25]. The $CuK_{\alpha 1}$ monochromatic radiation is provided by a bent germanium monochromator and the diffracted beams are simultaneously recorded using a curved position sensitive detector with a 120° aperture (CPS120—INEL-France). Such asymmetric geometry under fixed incidence is particularly suitable for surface characterisation and thin film structure analysis. The incident angle was fixed to about 4–7° in order to favour the irradiated volume without impairing the resolution, i.e. without an excessive broadening of the X-ray diffraction line profile.

Results

LSM precursor coatings deposited on (100) Si single crystal wafers have been synthesised from various initial metallic salt concentration sols, ranging from 0.08 to 0.6 mol/l. After a drying at 100 °C, the films are continuous, transparent, homogeneous and crack free as observed by optical microscopy. Before to be investigated by the different techniques previously presented which give additional information on microstructure, orientation and morphological characteristics of the layers, they are annealed at 700 °C during 2 h in order to remove the residual organics and to obtain the crystallisation of the amorphous precursors [13].

X-ray reflectivity curves of these coatings and uncoated Si substrate are presented in Fig. 2 and first analysed. Most of the reflected intensity curves corresponding to the LSM thin films present well marked oscillations, known as Kiessig fringes [26], which are significant of continuous, homogenous and uniform layers with low surface and interface roughnesses (Fig. 2). When the metallic salt concentration

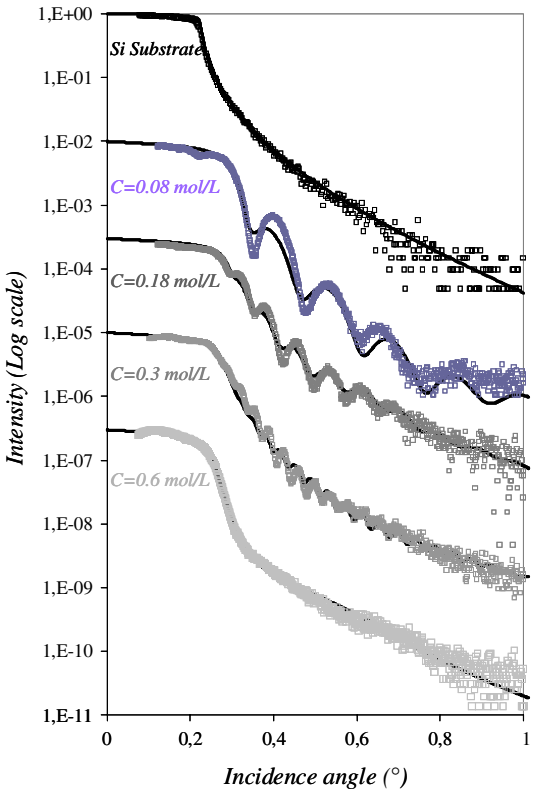

Fig. 2 X-ray reflectivity curves for silicon wafer and LSM thin films for C ranging from 0.08 to 0.6 mol/l after heat treatment during 2 h at 700 °C in air. Full lines are the best fits calculated from the recursive Parratt formalism

increases, both the position of the critical angle and the period of the interference fringes decrease. This behaviour points out that the layers density decreases while the layers thickness increases. However, for C = 0.6 mol/l, no periodic oscillations are observed because the film is probably too thick according to the reflectometer resolution. Indeed, it can be considered as an infinite medium for the X-ray beam. Nevertheless, its thickness has been determined by using an optical profilometer (Zygometer) operating as a Perrot-Fabry interferometer [10].

The intensity of the reflected beam by the uncoated Si single crystal substrate shows a monotonous decrease when the X-ray beam incident angle α increases, in good agreement with the classical evolution for a dioptre separating two media of different electronic densities. Furthermore, the measured critical angle corresponding to total reflection, $\alpha_c = 0.224°$, is in very good agreement with the theoretical value of 0.226° [27]. For fitting the right above presented thin LSM coating experimental XXR curves with the Parratt formalism model, the silicon substrate refraction index is fixed accordingly to its theoretical value and the refined parameters only concern the thin film microstructure, i.e. thickness, index of refraction, surface and interface roughnesses.

On Fig. 2, the continuous lines correspond to the best fitting curves from which the microstructural parameters are deduced. To reach such experimental and calculated curves agreement, we assume that films are constituted of two layers. For all films, an additional top-layer of only few nanometers, in a 1–10 nm range, with a density slightly lower than the one observed for the inner coat is added.

The thickness and the density of the inner layer are displayed in Fig. 3 as a function of the initial metallic salt concentration in the sol. The layer thickness, e, versus the initial metallic salt concentration, C, increases from 25 to 230 nm for C = 0.08 and 0.6 mol/l, respectively, and varies according to a power law with an exponent value superior to one, $e \sim C^{1.26}$. The density of the layer as estimated through its refractive index continuously decreases when the initial metallic salt concentration increases. In other words, the layers porosity slightly increases with the initial metallic salt concentration and the occupied volume, for an equivalent mass of oxide deposited, is more important for a sol of high concentration leading to a lower density. Finally, the root means square (r.m.s.) roughness parameters, about 0.5–1.5 nm for each interface, are in the same range order than the one measured for Si single crystal substrate.

XRD analyses performed on these annealed films show that they are crystallised in the pure perovskite form. For example, the XRD pattern collected for the thicker film is presented in Fig. 4. The peak positions and intensities are similar to those observed on LSM powders elaborated in the same conditions as reported in previous work [28]. These LSM powders crystallise in the rhombohedral symmetry of the perovskite and index in the R_{-3c} space group. Accordingly, for all films,

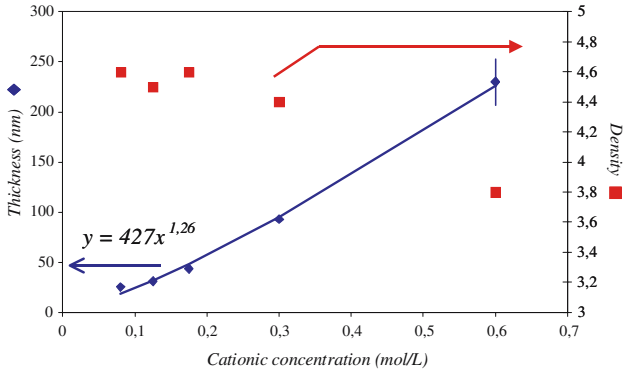

Fig. 3 Both thickness and density evolutions of LSM/Si thin films after heat treatment during 2 h at 700 °C versus metallic salt concentration

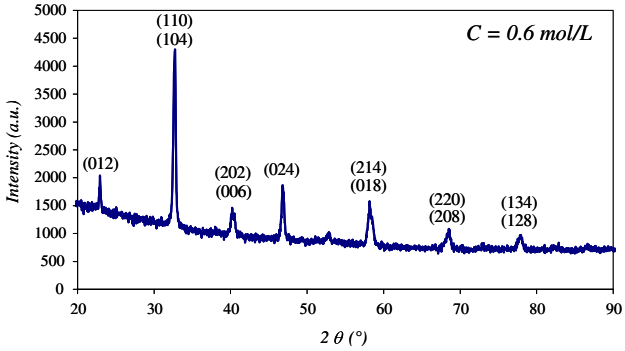

Fig. 4 X-ray diffraction pattern of LSM/Si thin film synthesised with C = 0.6 mol/l and fired at 700 °C during 2 h

XRD spectra are indexed in the $R_{\bar{3}c}$ system. This result shows that the thin solid films are polycrystalline and as the relative intensities are in good accordance with data of the JCPDS file, N° 82-1152, the LSM nanocrystals have random orientations in respect to the Si single crystal substrate.

Finally, GISAXS measurements are performed. We remind that SAXS experiments which are commonly used in the transmission mode provide numerous microstructural information on scattering entities on a nanometric scale and have been extensively described [29, 30]. However, when the heterogeneities of electronic density occur at the vicinity of a material surface or in a thin layer as it is the case for the LSM sol–gel layers, the use of grazing incidence is the best experimental configuration as it was demonstrated by Levine et al. [21, 31]. The principle of such GISAXS experimental technique which combines both X-ray reflectometry and small-angle X-ray scattering theory has been fully described by Naudon and Thiaudière [20].

With the GISAXS geometry, the X-ray path inside the thin layer is considerably increased, the signal-to-background ratio improved and the intrinsic scattering of the substrate suppressed. Due to the very small X-ray beam incidence angle, the illuminated area of finite size sample is assumed to be constant and the X-ray irradiated sample volume is only a function of the X-ray penetration depth, which is directly linked to the incidence angle [20]. Per contra, the accessible 2θ angular domain, where the scattering signal could be recorded, is obviously limited. The larger the incidence angle, the less the 2θ angular domain. Therefore, the choice of the incidence angle is crucial and the key point of GISAXS experiments. It must be set to a value obviously higher than the critical angle while ensuring the better resolution-intensity compromise.

The GISAXS measurements are done on the denser LSM layer, which maybe presents the smallest particle size and interparticles distance. Indeed, it corresponds to the lowest initial metallic salt concentration of 0.08 mol/l. Its critical angle and its thickness are about 0.32° and only 25 nm, respectively, after heat treatment at 700 °C during 2 h. Consequently, the X-ray beam incidence angle is set to 0.4° with respect to the layer surface, a value higher than the critical angle, allowing the irradiation of the whole layer and ensuring the better resolution-intensity compromise. The resulting scattered intensity curve, I(q), exhibits a maximum located at a scattering vector, q_m, different from 0 (Fig. 5). Such pattern feature indicates the existence of a correlation length, ξ, in the plane of the layer which can be deduced from the position of the intensity maximum q_m by $\xi = 2\pi/q_m$ and is found to be about 15 nm [30]. In the large-q domain, the scattered intensity, plotted in a Ln–Ln scale, decreases according to a power law with an exponent near to –4 (Fig. 5). This behaviour, known as the Porod law [29, 30], points out that the crystallised LSM nanoparticles are homogeneous with a well-defined smooth surface.

Discussion

On the one hand, the conventional electrolyte material for SOFC applications is Yttrium Stabilised Zirconia (YSZ). However, the surface roughness of the polished polycrystalline YSZ substrates does not allow scattering measurements such as X-ray reflectometry. Indeed, such substrate surface roughness will involve same range order surface and interface roughnesses for the deposited thin film [11, 12] leading to both an exponential decrease of reflected intensity and a large attenuation of the interference fringes on the XRR curves [16, 19]. Besides, parasite diffusion as Yoneda peaks [32] can be observed and disturbs the GISAXS measurements [33].

On the other hand, in the dip-coating process, the deposited film thickness, e, is that which balances the viscous drag and gravity force [15, 34]:

$$e = c\sqrt{\eta U_0/\rho g} \quad (1)$$

where c is close to 0.8 for Newtonian liquids, η, ρ, U_0, and g are the sol viscosity and the density, the withdrawal speed and the gravity, respectively. Therefore, in the sol–gel route, the control of the layer thickness may be easily achieved by modifying synthesis parameters including viscosity, withdrawal speed, concentration of metallic salts in the polymeric sol, heat treatment, etc... [14, 15, 35, 36]. For low substrate withdrawal speed and liquid viscosity, this balance is

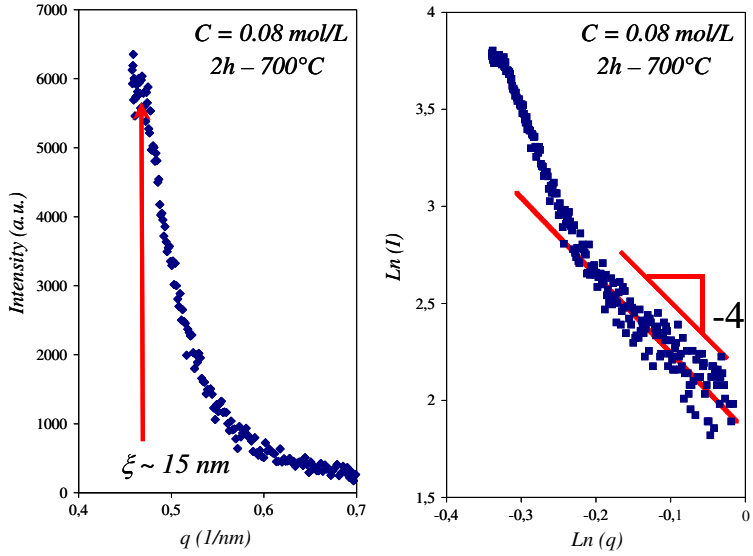

Fig. 5 GISAXS curve of LSM thin film synthesised with C = 0.08 mol/l after thermal treatment at 700 °C during 2 h on both a linear and bi-logarithmical scales

modulated by the ratio of viscous drag to liquid–vapour surface tension, γ_{LV}, according to the relationship derived by Landau and Levich:

$$e = 0.94(\eta U_0)^{2/3}/\gamma_{LV}^{1/6}(\rho g)^{1/2} \quad (2)$$

In both cases, the raw coating thickness mainly depends on the withdrawal speed and the viscosity of the liquid while the final thickness of the annealed coating will also rely on the solid content. Consequently, the substrate chemical nature does not have, in a first approximation, a major effect on the deposited layers thickness.

Thus, according to Eqs. 1 and 2, we have used (100) silicon single crystal wafers instead of polished polycrystalline YSZ substrates by assuming that the thickness of the deposited layer on polycrystalline YSZ substrates will be the same than those observed on Si single crystals and that the results will be transposable to a certain extent. In this way, the experimental difficulties encountered by using polycrystalline YSZ substrates, i.e. the roughness effects on the X-ray scattering measurements, are also solved.

The effect of the metallic salt concentration on the thickness and the microstructure of LSM layers elaborated via a polymeric method is then studied. The LSM thin films are elaborated on Si substrates from sols whose metallic salt concentration ranges from 0.08 to 0.6 mol/l, their viscosity and the withdrawal speed being kept constant and equal to 40 mPa·s and 1.7 cm/min, respectively. The raw as well as the annealed coatings are homogeneous, transparent and crack-free. Before annealing, the film thickness is nearly constant and independent of the initial metallic salt concentration as observed in a previous study [10]. According to this result and to Eqs. 1 or 2, the deposited coating thickness is concluded to be mainly managed by the sol HMTA content.

After thin coating annealing at 700 °C for 2 h, the collected experimental X-ray reflectivity data are better simulated by introducing a smaller density cap layer of only few nanometers upon the main denser layer. Such behaviour has already been observed for zirconia thin films elaborated by the sol–gel process and reported by Rizzato et al. [37]. However, some slight discrepancies between the experimental and calculated XXR curves remain yet. By considering that LSM thin films are composed of only two layers, the fitting model is probably too simple to fully describe the coating microstructure which is almost certainly more complex.

In particular, it is known that the appearance of an interfacial layer between the deposited coating and Si substrate is unavoidable during firing. The growth of such underlying layer has been widely studied versus numerous parameters such as chemical nature of the deposited coating, oxygen partial pressure, annealing conditions and so on [38–40]. According to the involved mechanism, silicon oxidation or interfacial reactions, the formation of intermixing or silicate phases as well as SiO_x or SiO_2 is generally observed. Nevertheless, in regards with their very low measured thickness, less than 5 nm at moderate annealing temperature [38] and an expected refractive index very close to the Si substrate one, we think that the taking into account of such underlying layer could probably improve slightly the XRR curve fitting but has no major impact on the measured density of the LSM layer as well as its thickness, the main microstructural parameters we are interesting in. A better fit of the XRR curves remains always conceivable by using more

complex layer models provided that they are established on relevant information from other experimental techniques such as cross-sectional high resolution transmission electronic microscopy which could probably be useful.

Thus, the refined thickness of the annealed LSM films is a function of the metallic salt concentration introduced in the polymeric sol. On the one hand, this thickness varies according to a power law with an exponent value of 1.26 and ranges from 25 to 230 nm for C = 0.08 and 0.6 mol/l, respectively. As the thickness of unannealed films, mainly managed by the sol HMTA content, is constant and independent of the initial metallic salt concentration, such exponent value, greater than 1, is significant of an increase of the porosity with the metallic salt concentration. On the other hand, XRD investigation made on heat-treated films reveals the crystallisation of the precursors coating in the single pure LSM perovskite phase. Consequently, the film density is easily evaluated through the refined refractive index from the X-ray reflectivity curves [11]. This density decreases with the initial metallic salt concentration in the sol in agreement with the thickness evolution. Thus, the higher the metallic salt concentration, the higher the thickness of the film and the more porous the film. Finally, both the surface and interface roughnesses are about 1 nm, which is equivalent to the evaluated Si single crystal substrate roughness (0.7 nm). These X-ray reflectivity results are in a certain extend similar to those observed for layers synthesised via other techniques such as CVD and PVD [41, 42].

The grazing incidence X-ray scattering signal, collected on the denser LSM layer, i.e. corresponding to the lowest initial metallic salt concentration of 0.08 mol/l, is assigned to the LSM nanocrystals [11, 12]. The sharp interference peak is significant, on the one hand, of a very homogeneous and narrow distribution of crystallised LSM nanoparticle sizes in the plane and, on the other hand, that the LSM nanocrystals self-organise in a relatively dense close-packed microstructure in agreement with the rather high density of this layer as measured by X-ray reflectivity. In such paracrystalline lattice model [43], the correlation length ξ corresponds to the nearest-neighbour distance. Since the end of the organics removal, at about 500 °C [10], the LSM nanocrystals are obviously in contact and the nearest-neighbour distance is assimilated to LSM nanocrystals size, which is about 15 nm for an annealing at 700 °C for 2 h. The Porod law being obeyed [29, 30], the LSM nanocrystals are homogeneous with a well-defined smooth surface and have a random orientation in respect to the Si single crystal substrate as revealed by the X-ray diffraction measurements. Therefore, this annealed coating is constituted by randomly oriented LSM nanocrystals, about 15 nm in size, which organise in a relatively dense close-packed microstructure. This microstructure is also evidenced and confirmed by Scanning Electron Micrograph (SEM) of the surface of this thin layer (Fig. 6).

The slight porosity increase, about 10–15%, when the initial metallic salt concentration increases could be explained by considering the corresponding bulk xerogels synthesised and annealed with the same experimental protocol. As it is always observed for sol–gel technology, the LSM nanocrystals size varies, on the one hand, according to the initial metallic salt concentration [10]. On the other hand, during the dipping, the liquid film runs out on the substrate, adheres to its surface and the evaporation of solvents leads to its rapid solidification. The as-prepared layer could be considered as a xerogel obtained by a concentration effect [11, 12]. Therefore, the LSM nanocrystal size variation versus the initial metallic salt concentration may change to some extent their stacking leading to a more or less dense close-packed microstructure.

All these results are obtained on Si single crystal substrates whereas the conventional electrolyte material for SOFC applications is YSZ. Thus, thin films of LSM on YSZ polished substrates are synthesised using the same synthesis parameters. Due to their intrinsic roughness, such substrates prevent especially the XRR and GISAXS measurements. The LSM layers are homogeneous, transparent and crack-free. As investigated by X-ray diffraction and scanning electron microscopy, respectively, the annealed films are crystallised in the single pure perovskite form and their microstructure features are quite similar to those

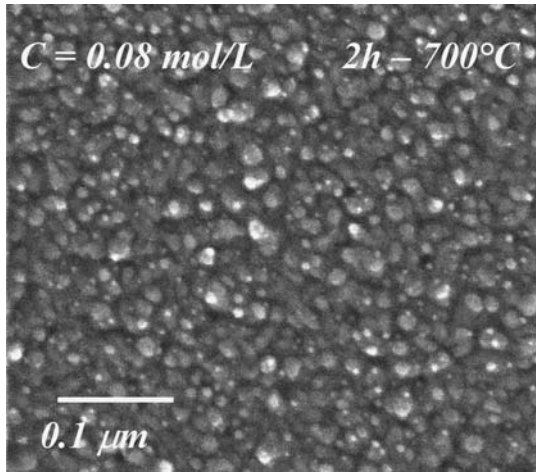

Fig. 6 SEM micrograph of LSM/Si thin film synthesised with C = 0.08 mol/l and fired at 700 °C during 2 h

previously detailed for Si substrates. Thus, the chemical nature of the substrate, Si single crystal or polycrystalline YSZ substrates, does not considerably influence the structure and microstructure of annealed films provided that the deposited films are thick enough. Such outcomes have been previously observed in other layer/substrate chemical couples and more particularly for sol–gel derived zirconia (ZrO_2) thin films deposited by a dip-coating process, on various substrates such as silica based glass, silicon and sapphire polish mirror single crystal substrates [44].

With the SOFC applications in aim, we now mainly focus this study on the synthesis of films with a metallic salt concentration of C = 0.6 mol/l which leads to the formation of the thickest and the most porous layer, a microstructure which is expected to favour the O_2 gas transportation to the triple phase boundaries. After calcination at 1,000 °C for 2 h in order to stabilise the material microstructure, the SEM micrographs show that the fired film is no longer continuous and exhibits both small pores and small solid phase islands (Fig. 7a). The resulting microstructure is very fine and seems well self-organised by presenting an order on a short length scale with a homogeneous distribution of islands size. Their correlation length is more precisely determined by using an image processing of the SEM micrograph, which allows the computation of the power spectrum or the square modulus of the Fourier transform (Fig. 8) [45]. A scattering ring centred on the reciprocal space origin is observed and similar to the X-ray scattering curve obtained at lower temperature (Fig. 5). The distribution of the intensity, evaluated from an integration of the scattered intensity on all directions of the reciprocal space, shows a well-defined maximum around 3 μm^{-1} corresponding to a preferential correlation length of about 330 nm in the film surface.

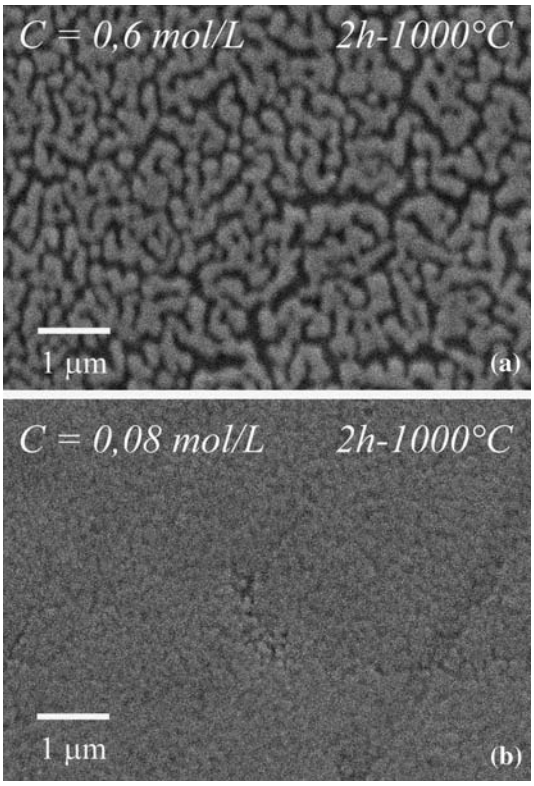

Fig. 7 SEM micrographs of LSM/YSZ thin films annealed at 1,000 °C during 2 h and synthesised with C = 0.6 mol/l (**a**) and C = 0.08 mol/l (**b**)

These kinds of particle growth and pore coarsening leading to this well known islanding or dewetting of the substrate and the associated mechanisms have been widely investigated for various layer/substrate chemical couples [36, 46–49]. These studies conclude that one of the main parameters governing the dewetting is the existence of a critical layer thickness, for fixed annealing conditions, and that the islanding could be avoided by optimising the initial layer thickness. In our case, the critical layer thickness could be found by varying the metallic salt concentration. Continuous and homogeneous layers are recovered, even for an annealing at 1,000 °C for 2 h, by decreasing the metallic salt concentration. An example of resulting microstructure is displayed in Fig. 7b for an initial metallic salt concentration of 0.08 mol/l.

The elaboration of electrodes for SOFC devices with a controlled porosity is critical for good performances of the system. The reduction of the oxygen at the triple boundary points (air/electrode/YSZ) depends both on composition and microstructure of the cathode [4, 50]. Sasaki et al. [51] reported that both the overvoltage and the ohmic loss at the triple boundary points for cathode materials are mostly affected by the electrode microstructure. Our results show that nanocrystallised LSM films with different porosities can be synthesised by controlling the initial metallic salt concentration of the polymeric sols. Indeed, several densities have been achieved from 50 to 70% of the theoretical density of LSM with metallic salt concentrations ranging from 0.08 to 0.6 mol/l. The measured coating thickness which is relatively weak for SOFC applications does not matter since the sol–gel process easily allows thick film synthesis by multi-layered film preparation with or without intermediate heat treatments.

Conclusion

Continuous, homogeneous and crack-free $La_{0.8}Sr_{0.2}MnO_3$ thin films are successfully synthesised by a sol–gel dip-coating method. Their structure and

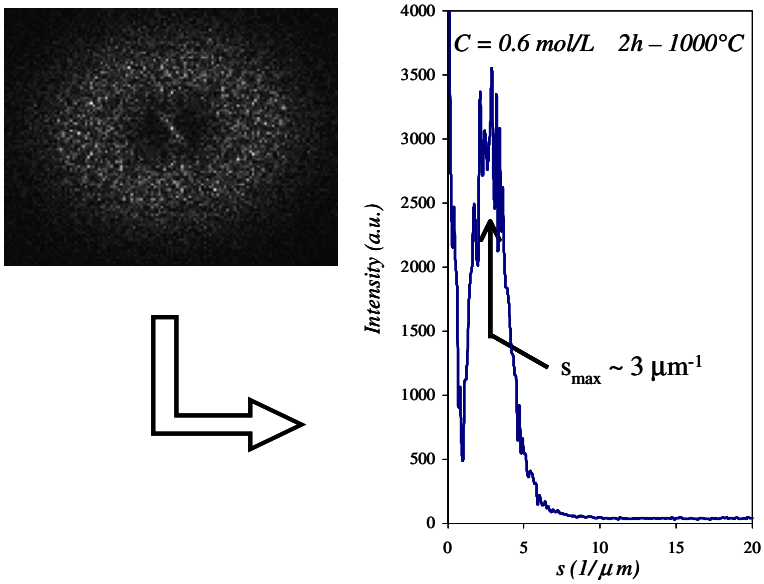

Fig. 8 Power spectrum of SEM micrograph of LSM/YSZ thin film, annealed at 1,000 °C during 2 h and synthesised with C = 0.6 mol/l, displayed in Fig. 7 and the corresponding intensity distribution integrated on the whole scattering ring, $s = 1/\xi$

microstructure versus the metallic salt concentration in the sol are fully characterised by using several complementary non-destructive X-ray scattering methods such as X-ray reflectivity, X-ray diffraction and grazing incidence small angle X-ray scattering. After annealing at 700 °C in air, the layer microstructure is composed of randomly oriented nanocrystallised LSM particles. Their narrow size distribution allows their self-stacking in a relatively dense close-packed microstructure. These characteristics are still preserved even after calcination at 1,000 °C for 2 h and seem to be independent of the nature of the substrate.

Correlations between the thickness, the density of the film and the metallic salt concentration in starting sol are established. The higher the ionic concentration, the higher the thickness and the more porous the microstructure. The control of processing parameters including concentration of metallic salts and the heat treatment conditions allows the elaboration of thin films with various porosities and thickness. This thin film porosity and thickness management is an advantage for further SOFC applications because they induce the polarisation resistance at the air/cathode/electrolyte interface by optimising the triple phase boundary lines.

Acknowledgements The authors acknowledge ADEME and the French Fuel Cell Network for their financial supports.

References

1. Nguyen MQ (1993) J Am Ceram Soc 76:563
2. Stevens P, Novel-Cattin F, Hammou A, Lamy C, Cassir M (2000) Techniques de l'ingénieur D5:3340
3. Van Roosmalen JAM, Huijsmans JPP, Plomb L (1993) Solid State Ionics 66:279
4. Kamata H, Hosuka A, Mizusaki J, Tagawa H (1998) Solid State Ionics 106:237
5. Bell RJ, Millar GJ, Drennan J (2002) Solid State Ionics 131:211
6. Van Roosmalen JAM, Huijsmans JPP, Cordfunke EHP (1991) In: Grosz F, Zegers P, Singhal SC, Yamamoto O (eds) Proceeding of 2nd international symposium on solid oxide fuel cells. Luxembourg, p 507
7. Chick LA, Pederson LR, Maupin GD, Bates JL, Thomas LE, Exarhos GJ (1990) Mater Lett 10
8. Chakraborty A, Sujatha Devi P, Roy S, Maiti HS (1994) J Mater Res 9:986
9. Pechini P (1967) Patent, 3.330.697 July 11
10. Gaudon M (2002) Ph.D. Thesis, Toulouse
11. Lenormand P (2001) Ph.D. Thesis, Limoges
12. Lenormand P, Lecomte A, Dauger A, Mary C, Guinebretière R (2000) J Phys IV 10:255
13. Gaudon M, Laberty-Robert C, Ansart F, Stevens P, Rousset A (2002) Solid State Sci 4:125
14. Gaudon M, Laberty-Robert C, Ansart F, Stevens P, Rousset A (2002) J New Mat Electrochem Syst 5:57
15. Brinker JF, Scherrer GW (1990) Sol–gel science. Academic Press Inc
16. Croce P, Névot L, Pardo B (1972) Nouv Rev D'Opt Appl 3:37
17. Naudon A, Chihab J, Goudeau P, Mimault J (1989) J Appl Cryst 22:460
18. Parratt LG (1954) Phys Rev 95:359
19. Névot L, Pardo B, Corno J (1988) Rev Phys Appl 23:1675
20. Naudon A, Thiaudière D (1997) J Appl Cryst 30:822
21. Levine JR, Cohen JB, Chung YW, Georgopoulos P (1989) J Appl Cryst 22:528
22. Naudon A, Babonneau D (1997) Z Metallkd 88:596
23. Babonneau D, Naudon A, Cabioc'h T, Lyon O (2000) J Appl Cryst 33:437
24. Kutsch B, Lyon O, Schmitt M, Mennig M, Schmidt H (1997) J Appl Cryst 30:948
25. Masson O, Guinebretière R, Dauger A (1996) J Appl Cryst 29:540
26. Kiessig H (1931) Ann Phys 10:769

27. Henke BL, Gullikson EM, Davis JC (1993) Atomic Data Nuclear Data 54:181
28. Lenormand P, Laberty-Robert C, Ansart F (2002) In: Proceedings of the France-Deutschland fuel cell conference, p 248
29. Guinier A, Fournet G (1955) Small-angle scattering of X-rays. John Wiley & Sons, Inc., NewYork
30. Glatter O, Kratky O (eds) (1982) Small-angle X-ray Scattering. Academic Press, London
31. Levine JR, Cohen JB, Chung YW (1991) Surf Sci 248:215
32. Yoneda Y (1963) Phys Rev 131:2010
33. Babonneau D (1999) Ph.D. Thesis, Poitiers
34. Brinker CJ, Hurd AJ, Schunk PR, Frye GC, Ashley CS (1992) J Non Cryst Sol 147&148:424
35. Lange FF (1996) Science 273:903
36. Miller KT, Lange FF (1989) Mater Res Soc Symp Proc 155:191
37. Rizzato AP, Santilli CV, Pulcinelli SH (1999) J Non-Cryst Solids 247:158
38. Copel M, Carlier E, Gusev EP, Guha S, Bojarczuck N, Poppeller M (2001) Appl Phys Lett 78:2670
39. Stemmer S, Chen Z, Keding R, Maria JP, Wicaksana D, Kingon AI (2002) J Appl Phys 92:82
40. Busch BW, Pluchery O, Chabal YJ, Muller DA, Opila RL, Raynien Kwo J, Garfunkel E (2002) MRS Bull 27:206
41. Holy V, Kubena J, Ohlidal I, Lischka K, Plotz W (1993) Phys Rev B 47:15896
42. Jergel M, Holy V, Majkova E, Luby S, Senderak R (1997) J Appl Cryst 30:64
43. Matsuoka H, Tanaka H, Hashimoto T, Ise N (1987) Phys Rev B 36:1754
44. Lenormand P, Lecomte A, Babonneau D, Dauger A (2006) Thin Solids Films 495:224
45. Boulle A (2002) Ph.D. Thesis, Limoges
46. Miller KT, Lange FF, Marshall DB (1990) J Mater Res 5:151
47. Seifert A, Vojta A, Speck JS, Lange FF (1996) J Mater Res 11:1470
48. Mary C, Guinebretière R, Trolliard G, Soulestin B, Villechaise P, Dauger A (1998) Thin Solids Films 336:156
49. Guinebretière R, Bachelet R, Boulle A, Masson O, Lecomte A, Dauger A (2004) Mater Sci Eng B 109:42
50. Kleitz M, Petitbon F (1996) Solid State Ionics 92:65
51. Sasaki K, Wurthe JP, Godickemeier M, Mitterdorfer A, Gauckler LJ (1995) In: Dokiya M, Yamamoto O, Tagawa H, Singhal SC (eds) Proceedings of the 4th Int. Symp. On SOFC, Yokohama, Japan, p 625